# TURBULENT IMPINGING JET INTO A POROUS BED WITH THERMAL NON-EQUILIBRIUM. PART1. POROUS LAYER THICKNESS EFFECT

**Felipe Tannús Dórea, dorea@ita.br**
**Marcelo J. S. de Lemos, delemos@ita.br**
Departamento de Energia - IEME
Instituto Tecnológico de Aeronáutica - ITA
12228-900 - São José dos Campos - SP, Brazil

***Abstract.*** *This work shows numerical results for a turbulent impinging jet against a flat plane covered with a layer of porous material considering the thermal non-equilibrium, using two macroscopic equations of energy: One for the fluid and another for the solid without considering the local thermal equilibrium, in turbulent regime by using numerical simulations. Macroscopic time-averaged equations for mass and momentum are obtained based on a concept called double decomposition, which considers spatial deviations and temporal fluctuations of flow properties. Turbulence is handled with a macroscopic k–e model, which uses the same set of equations for both the fluid layer and the porous matrix. The numerical technique employed is the control volume method in conjunction with a boundary-fitted coordinate system. One unique computational grid is used to compute the entire heterogeneous medium. The SIMPLE algorithm is applied to relax the system of algebraic equations. The effect of porus layer thickness in the energy model on the local distribution of Nusselt number and in Integral wall heat flux was analyzed. Results indicates that for thinner porous layer a substantially diferent Nusselt number is calculated and the integral heat flux for two models of energy is diferent for all range of properties tested, also a presence of a porous layer is beneficial for* $\phi = 0.95$, $k_s/k_f = 10$ *and* $h/H < 0.5$, *since in this conditions the ratio* $q_w^{\phi}/q_w$ *is greater than 1.*

***Keywords****: Impinging Jet,Turbulence,Porous Media, Thermal Non-Equilibrium*

## 1. INTRODUCTION

Turbulent impinging jets are commonly used in industrial applications with the objective of obtaining effective heating, cooling or drying processes. The main advantage of using impinging jets is the possibility to obtain highly localized mass and heat transfer rates due to thin boundary layer, hydrodynamics and thermal

One knows that by increasing the contact area between the coolant and the surface, larger amounts of heat can be extracted subjected to the same temperature difference. For example, such heat-sink devices are commonly used in the microcomputer industry to enhance the extraction of heat from ever-smaller microprocessors. Accordingly, porous metal foams conveniently installed over hot surfaces can enhance heating/cooling process due to their high volumetric surface area (interfacial area per unit volume).

The objective of the present contribution is to extend the investigation of Fischer and de Lemos (2008) which made use on One-Energy equation model (1EEM) also referred to as the Local Thermal Equilibrium model (LTE), to a heat transfer analysis applying now a Two-Energy Equation model (2EEM), also referred to as Local Thermal Non-Equilibrium model- (LTNE). Both sets of results are compared in order to access the performance of each model and to evaluate under which circumstances the addition of a porous layer made of thermal conducting material can enhance the overall heat transferred from a flat surface under an impinging jet.

## 2. PROBLEM DESCRIPTION

The geometries and nomenclature of the problem are presented in detailed form in Figure 1. A turbulent jet with uniform velocity $v_o$ and constant temperature $T_o$ enters through a gap into a channel with height $H$ and length $2L$. Fluid impinges normally against the bottom plate yielding a two-dimensional confined impinging jet configuration. The width of the inlet nozzle is $B$ and the bottom plate temperature, $T_1$, is maintained constant and 38.5K above the temperature of the incoming jet, $T_o$. In a different configuration, the bottom surface is covered with a porous layer of height $h$ (Figure 1*b*). In both cases, the flow is assumed to be two-dimensional, turbulent, incompressible and steady. Also, the porous medium is taken to be homogeneous, rigid and inert. Fluid properties are constant and gravity effects are neglected.

The boundary conditions for the problem are: a) constant velocity and temperature profiles of the entering jet, b) no slip condition on the walls, c) symmetry condition in $x = 0$, d) fully developed flow at channel exit ($x = L$). At the bottom plate ($y = H$), constant temperature condition is assumed whereas along the upper wall, for $B/2 < x \le L$, null heat flux condition prevails.

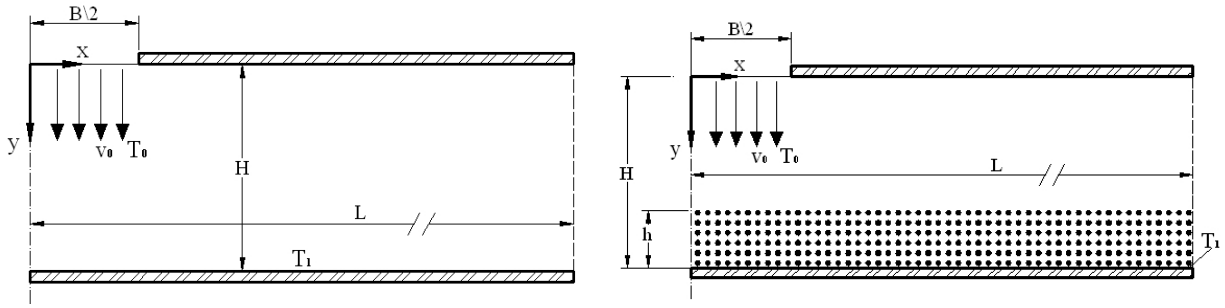


(a) (b)

Figure 1– Cases Investigated (a) Clean Medium (b) Porous Medium

## 3. MATHEMATICAL MODELING

The most of theoretical development is readily available in the open literature, the governing equations will be just presented and details about their derivations can be obtained in the mentioned papers. Essentially, local instantaneous equations are volume-averaged using appropriate mathematical tools. Accordingly for turbulent flow, the equations read:

**Macroscopic continuity equation**

The macroscopic equation of continuity for an incompressible fluid flowing through a porous medium is given by:

$$\nabla \cdot \overline{\mathbf{u}}_D = 0 \tag{1}$$

where, $\overline{\mathbf{u}}_D = \phi \langle \overline{\mathbf{u}} \rangle^i$ and $\langle \overline{\mathbf{u}} \rangle^i$ identifies the intrinsic (liquid) average of the time-averaged velocity vector $\overline{\mathbf{u}}$

**Macroscopic momentum equation:**

The macroscopic momentum equation (Navier-Stokes) for an incompressible fluid with constant properties ($\rho$ and $\mu$ constants) flowing through a porous medium, can be written as:

$$\rho\left[\frac{\partial \overline{\mathbf{u}}_D}{\partial t} + \nabla \cdot \left(\frac{\overline{\mathbf{u}}_D \overline{\mathbf{u}}_D}{\phi}\right)\right] = -\nabla(\phi \langle \overline{p} \rangle^i) + \mu \nabla^2 \overline{\mathbf{u}}_D - \nabla \cdot (\rho \phi \langle \overline{\mathbf{u}'\mathbf{u}'} \rangle^i) - \left[\frac{\mu \phi}{K} \overline{\mathbf{u}}_D + \frac{c_F \phi \rho |\overline{\mathbf{u}}_D| \, \overline{\mathbf{u}}_D}{\sqrt{K}}\right] \tag{2}$$

where the last two terms in equation (2) represent the Darcy and the Forchheimer terms, respectively. The symbol *K* is the porous medium permeability, $c_F$ = 0.55 is the form drag coefficient (Forchheimer coefficient), $\langle \overline{p} \rangle^i$ is the intrinsic average pressure of the fluid and $\phi$ is the porosity of the porous medium.

The macroscopic Reynolds stress, $-\rho \phi \langle \overline{\mathbf{u}'\mathbf{u}'} \rangle^i$, appearing in Eq. (2) is given as,

$$-\rho \phi \langle \overline{\mathbf{u}'\mathbf{u}'} \rangle^i = \mu_{t_\phi} 2 \langle \overline{\mathbf{D}} \rangle^{\mathbf{v}} - \frac{2}{3} \phi \rho \langle k \rangle^i \mathbf{I} \tag{3}$$

where,

$$\langle \overline{\mathbf{D}} \rangle^v = \frac{1}{2}\left[\nabla(\phi \langle \overline{\mathbf{u}} \rangle^i) + [\nabla(\phi \langle \overline{\mathbf{u}} \rangle^i)]^T\right] \tag{4}$$

is the macroscopic deformation tensor, $\langle k \rangle^i = \langle \overline{\mathbf{u}' \cdot \mathbf{u}'} \rangle^i / 2$ is the intrinsic turbulent kinetic energy, and $\mu_{t_\phi}$, is the turbulent viscosity, which is modeled in Pedras and de Lemos (2001) similarly to the case of clear flow, in the form,

$$\mu_{t_\phi} = \rho c_\mu \frac{\langle k \rangle^{i^2}}{\langle \varepsilon \rangle^i} \tag{5}$$

The intrinsic turbulent kinetic energy per unit mass and its dissipation rate are governed by the following equations,

$$\rho\left[\frac{\partial}{\partial t}\left(\phi\langle k\rangle^i\right)+\nabla\cdot\left(\overline{\mathbf{u}}_D\langle k\rangle^i\right)\right]=\nabla\cdot\left[\left(\mu+\frac{\mu_{t_\phi}}{\sigma_k}\right)\nabla\left(\phi\langle k\rangle^i\right)\right]-\rho\langle\overline{\mathbf{u}'\mathbf{u}'}\rangle^i:\nabla\overline{\mathbf{u}}_D$$
$$+c_k\rho\frac{\phi\langle k\rangle^i|\overline{\mathbf{u}}_D|}{\sqrt{K}}-\rho\phi\langle\varepsilon\rangle^i \tag{6}$$

$$\rho\left[\frac{\partial}{\partial t}\left(\phi\langle\varepsilon\rangle^i\right)+\nabla\cdot\left(\overline{\mathbf{u}}_D\langle\varepsilon\rangle^i\right)\right]=\nabla\cdot\left[\left(\mu+\frac{\mu_{t_\phi}}{\sigma_\varepsilon}\right)\nabla\left(\phi\langle\varepsilon\rangle^i\right)\right]+c_1\left(-\rho\langle\overline{\mathbf{u}'\mathbf{u}'}\rangle^i:\nabla\overline{\mathbf{u}}_D\right)\frac{\langle\varepsilon\rangle^i}{\langle k\rangle^i}$$
$$+c_2c_k\rho\frac{\phi\langle\varepsilon\rangle^i|\overline{\mathbf{u}}_D|}{\sqrt{K}}-c_2\rho\phi\frac{\langle\varepsilon\rangle^{i\,2}}{\langle k\rangle^i} \tag{7}$$

where, $\sigma_k$=1, $\sigma_\varepsilon$=1.3, $c_1$=1.44, $c_2$=1.92, $c_\mu$=0.09 and $c_k$=0.28 are non-dimensional constants defined in Launder and Spalding (1974).

**Two Energy Equation Model**

The One Energy Equation model is usually valid when the temperature difference between the solid and fluid phase is relatively small. In this case, the condition of Local Thermal Equilibrium (LTE) is applied. When the LTE is far from reality, the one energy equation model needs to be replaced with the two energy equation model, which treats the solid and the fluid phase on separate, via their own macroscopic energy equations Saito and de Lemos (2005). Those equations read:

$$\left(\rho c_p\right)_f\left[\frac{\partial\phi\langle\overline{T_f}\rangle^i}{\partial t}+\nabla\cdot\left\{\phi\left(\langle\overline{\mathbf{u}}\rangle^i\langle\overline{T_f}\rangle^i+\underbrace{\langle{}^i\overline{\mathbf{u}}^{\,i}\overline{T_f}\rangle^i}_{\text{thermal disperson}}+\underbrace{\overline{\langle\mathbf{u}'\rangle^i\langle T_f'\rangle^i}}_{\text{turbulent heat flux}}+\underbrace{\langle\overline{{}^i\mathbf{u}'\,{}^iT_f'}\rangle^i}_{\text{turbulent thermal disperson}}\right)\right\}\right]=$$
$$\underbrace{\nabla\cdot\left[k_f\nabla\left(\phi\langle\overline{T_f}\rangle^i\right)+\frac{1}{\Delta V}\int_{A_i}\mathbf{n}_i\,k_f\,\overline{T_f}\,dA\right]}_{\text{conduction}}+\underbrace{\frac{1}{\Delta V}\int_{A_i}\mathbf{n}_i\cdot k_f\nabla\overline{T_f}\,dA}_{\text{interfacial heat transfer}} \tag{8}$$

where the expansion,

$$\langle\overline{\mathbf{u}'T_f'}\rangle^i=\langle\overline{(\langle\mathbf{u}'\rangle^i+{}^i\mathbf{u}')(\langle T_f'\rangle^i+{}^iT')}\rangle^i=\overline{\langle\mathbf{u}'\rangle^i\langle T_f'\rangle^i}+\langle\overline{{}^i\mathbf{u}'\,{}^iT_f'}\rangle^i \tag{9}$$

has been used in light of the double decomposition concept given by Pedras and de Lemos (2001). For the solid phase, one has,

$$\left(\rho c_p\right)_s\left\{\frac{\partial(1-\phi)\langle\overline{T_s}\rangle^i}{\partial t}\right\}=\underbrace{\nabla\cdot\left\{k_s\nabla\left[(1-\phi)\langle\overline{T_s}\rangle^i\right]-\frac{1}{\Delta V}\int_{A_i}\mathbf{n}_i\,k_s\overline{T_s}\,dA\right\}}_{\text{conduction}}$$
$$-\underbrace{\frac{1}{\Delta V}\int_{A_i}\mathbf{n}_i\cdot k_s\nabla\overline{T_s}\,dA}_{\text{interfacial heat transfer}} \tag{10}$$

where $\langle\overline{T_s}\rangle^i$ and $\langle\overline{T_f}\rangle^i$ denote the intrinsic average temperature of solid and fluid phases, respectively, $k_f$ and $k_s$ are the fluid and solid thermal conductivities, respectively. $A_i$ is the interfacial area within the REV and $\mathbf{n}_i$ is the normal unit vector at the fluid-solid interface, pointing from the fluid towards the solid phase.

**Interfacial Heat Transfer**

In Eq. (8) and Eq.(10) the heat transferred between the two phases can be modeled by means of a film coefficient $h_i$ such that,

$$h_ia_i\left(\langle\overline{T_s}\rangle^i-\langle\overline{T_f}\rangle^i\right)=\frac{1}{\Delta V}\int_{A_i}\mathbf{n}_i\cdot k_f\nabla\overline{T_f}\,dA=\frac{1}{\Delta V}\int_{A_i}\mathbf{n}_i\cdot k_s\nabla\overline{T_s}\,dA \tag{11}$$

where $a_i = A_i / \nabla V$ is the interfacial area per unit volume. In porous media, the high values of $a_i$ make them attractive for transferring thermal energy via conduction through the solid followed by convection to a fluid stream.

A numerical correlation for the interfacial convective heat transfer coefficient was proposed by Saito and de Lemos, for turbulent flow as:

$$\frac{h_i D}{k_f} = 0.08\left(\frac{Re_D}{\phi}\right)^{0.8} Pr^{1/3};\ \text{for } 1.0x10^4 < \frac{Re_D}{\phi} < 2.0x10^7\ \text{,valid for } 0.2 < \phi < 0.95\,, \tag{12}$$

Using the model shown in Eq. (11) above for the interfacial heat transfer $h_i$, and Eq.(12), the energy equations (8) and (10) can be rewritten as:

$$\left\{\left(\rho c_p\right)_f \phi\right\}\frac{\partial \langle \overline{T_f} \rangle^i}{\partial t} + \left(\rho c_p\right)_f \nabla \cdot \left(\mathbf{u}_D \langle \overline{T_f} \rangle^i\right) = \nabla \cdot \left\{\mathbf{K}_{eff,f} \cdot \nabla \langle \overline{T}_f \rangle^i\right\} + h_i a_i \left(\langle \overline{T_s} \rangle^i - \langle \overline{T_f} \rangle^i\right) \tag{13}$$

$$\left\{(1-\phi)\left(\rho c_p\right)_s\right\}\frac{\partial \langle \overline{T_s} \rangle^i}{\partial t} = \nabla \cdot \left\{\mathbf{K}_{eff,s} \cdot \nabla \langle \overline{T_s} \rangle^i\right\} - h_i a_i \left(\langle \overline{T_s} \rangle^i - \langle \overline{T_f} \rangle^i\right) \tag{14}$$

where, $\mathbf{K}_{eff,f}$ and $\mathbf{K}_{eff,s}$ are the effective conductivity tensor for fluid and solid, respectively, given by:

$$\mathbf{K}_{eff,f} = [\phi k_f]\,\mathbf{I} + \mathbf{K}_{disp} \tag{15}$$

$$\mathbf{K}_{eff,s} = [(1-\phi) k_s]\,\mathbf{I} \tag{16}$$

and $\mathbf{I}$ is the unit tensor.

**Non-dimensional parameters:**

The local Nusselt number for the one-energy equation model as used by Fischer and de Lemos (2010) :

$$Nu = \frac{-2H}{T_1 - T_0}\left(\frac{\partial \langle T \rangle^i}{\partial y}\right) \tag{17}$$

In Eq. 17 it is assumed the local thermal equilibrium assumption, i.e., $\langle T \rangle^i = \langle T_s \rangle^i = \langle T_f \rangle^i$ is also presented below for comparison between two closures here used. The longitudinal Nusselt number for two-energy equation model are calculated for both the fluid and solid phases and are defined as Alazami and Vafai (2000)

Fluid phase Nusselt number:

$$Nu_f = \frac{-2H}{T_1 - T_0}\left(\frac{\partial \langle T_f \rangle^i}{\partial y}\right) \tag{18}$$

Solid phase Nusselt number:

$$Nu_s = \frac{-2H}{T_1 - T_0}\left(\frac{\partial \langle T_s \rangle^i}{\partial y}\right) \tag{19}$$

## 4. NUMERICAL METHOD

Equations (1), (2), (13) and (14) subject to interface and boundary conditions were discretized in a two-dimensional control volume involving both clear and porous mediums. The equations discretization uses a system of generalized coordinates. The finite volumes method was used in the discretization and the SIMPLE algorithm (Patankar 1980) was used to the treatment of pressure-velocity coupling.

The Fig. 2 present a typical control volume together with the generalized coordinates system, $\eta - \xi$. The general and discretized form of the two-dimensional conservation equation of a generic property $\varphi$, in permanent regime, is given by:

$$I_e + I_w + I_n + I_s = S_\varphi \tag{20}$$

where $I_e$, $I_w$, $I_n$ and $I_s$ represent, respectively, the fluxes of $\varphi$ in the faces east, west, north and south of the control volume and $S_\varphi$ its term source.

Every time the source term is dependent of $\langle\varphi\rangle^i$ **,** it will be linearized in the following form:

$$S_\varphi \approx S_\varphi^{**}\langle\varphi\rangle_p^i + S_\varphi^* \tag{21}$$

The source terms in the momentum equations to $x$ direction are given by:

$$S^{*x} = \left(S_e^{*x}\right)_P - \left(S_w^{*x}\right)_P + \left(S_n^{*x}\right)_P - \left(S_s^{*x}\right)_P + S_P^* \tag{22}$$

$$S^{**x} = S_\phi^{**} \tag{23}$$

where, $S^{*x}$ is the diffusive part treated in explicit form. The term $S^{**x}$ in the equation for the porous medium is composed by the term of Darcy coefficient in the $x$ direction.

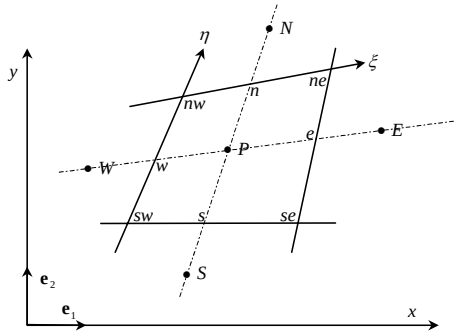


Figure 2 – Control volume and notation

## 5. RESULTS AND DISCUSSION

Low Reynolds $k-\varepsilon$ model was used. To ensure the modeling of the flow properties within the laminar sublayer the value of $y^+$ was kept less than or equal to 1, $(y^+ \le 1)$. The profile of turbulent kinetic energy $(k)$ at the entrance of the jet was calculated according to the equation:

$$k = \frac{3}{2}(v_0.T_i)^2 \tag{24}$$

where $v_0$ is the profile of inlet velocity in the channel and $T_i$ is the turbulent intensity. The profile of turbulent kinetic energy dissipation $(\varepsilon)$ is obtained by the equation:

$$\varepsilon = c_\mu^{\frac{3}{4}} \frac{k^{\frac{3}{2}}}{l} \tag{25}$$

Where $c_\mu$ is the constant of turbulence model described in the mathematical model, $k$ is the kinetic energy of turbulence and $l$ is the turbulence scale.

The fluid properties and the geometric dimensions (figure 1) used for all cases solved in turbulent flow presented are shown in the table below, the diameter used is $D = B$

Table 1 - Parameters used in turbulent flow

| Fluid | Especific Mass ( $\rho$ ) | Viscosity ( $\mu$ ) | $B$ | $L$ | $T_0$ | $T_1$ | Turbulence Scale | Turbulent Intensity |
|---|---|---|---|---|---|---|---|---|
| Air | 1,225 kg/m$^3$ | 1,789x10$^{-5}$ N.s/m$^2$ | 14.23 mm | 500 mm | 309.1 K | 347.6 K | 0.07B | 2% |

The results are compared with numerical results and experimental data, in the numerical results of Wang and Mujundar in Figure 3a and Figure 3b was used a two low Reynolds $k-\varepsilon$ models: One developed by Change, Hsieh and Chen, thereafter referred to as CHC as described in Chang et all (1995) and in Hsieh and Chang (1996) and the developed by Launder and Sharma thereafter referred to as LS as described in Launder and Sharma (1974). In all

numerical simulations were used an 80 x 216 (17280 nodes) grid, refined next to the walls. The grid and computational code validation for clean medium are made comparing the obtained results with literature data for two different configurations.

Figure 3a shows the distribution of the local Nusselt number close to the incidence inferior plate and it is compared with experimental data of Van Heiningen (1982) and numerical results of Wang and Mujumdar (2004) and Fischer and de Lemos (2010). The Reynolds number is $\mathrm{Re} = 5200$, the inlet velocity profile is fully developed for a flow between parallel plates Fox (1998), the temperature profile is uniform and the ratio between the nozzle-to-plate spacing and nozzle width is $H/B = 6$.

Figure 3b shows the comparison of local Nusselt number close to inferior plate with the experimental data of Van Heiningen (1982) and numerical results of Wang and Mujumdar calculated with two different models of turbulence and numerical results of Fischer and de Lemos (2010). The Reynolds number is $\mathrm{Re} = 10400$, the inlet velocity and temperature profiles are uniforms and the ratio between the nozzle-to-plate spacing and nozzle width is $H/B = 2.6$.

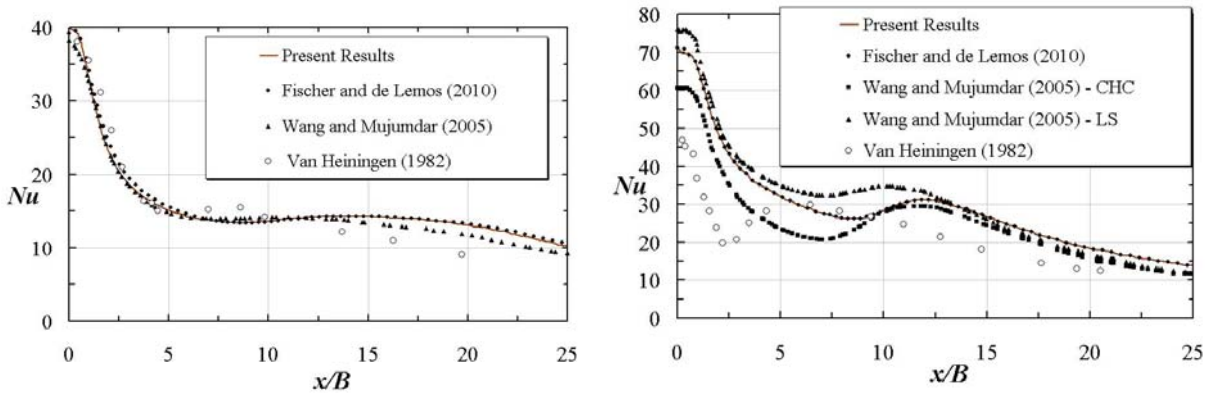


(a) (b)

Figure 3 – Distribution of Nusselt number throughout the inferior wall for a clean medium. (a) $H/B = 6$ (b) $H/B = 2.6$

All the following results have been simulated with the following geometric configurations and boundary conditions: uniform velocity and temperature profile; inlet jet temperature $T_1 = 309.1K$; the inferior plate temperature is maintained constant and equal to $T_o = 347.6K$; the ratio between the nozzle-to-plate spacing and nozzle width is maintained constant and equal to $H/B = 2.6$; the nozzle width is $B = 1\times10^{-03} m$.

Figures 4a,b and 5a,b, shows the flow behavior fields: 4(a) streamlines, 4(b) kinetic turbulent energy and thermal behavior fields: 5(a) fluid temperature and 5(b) solid temperature field for various porous thickness layer of porous bed.

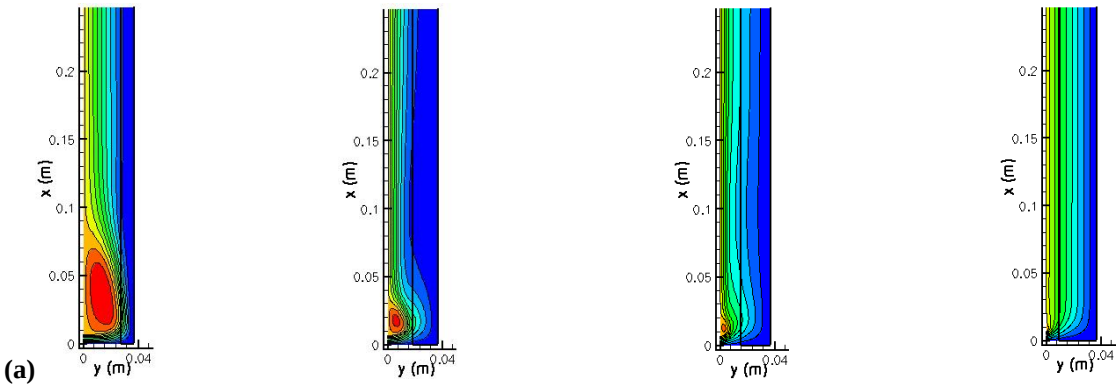


**(a)**

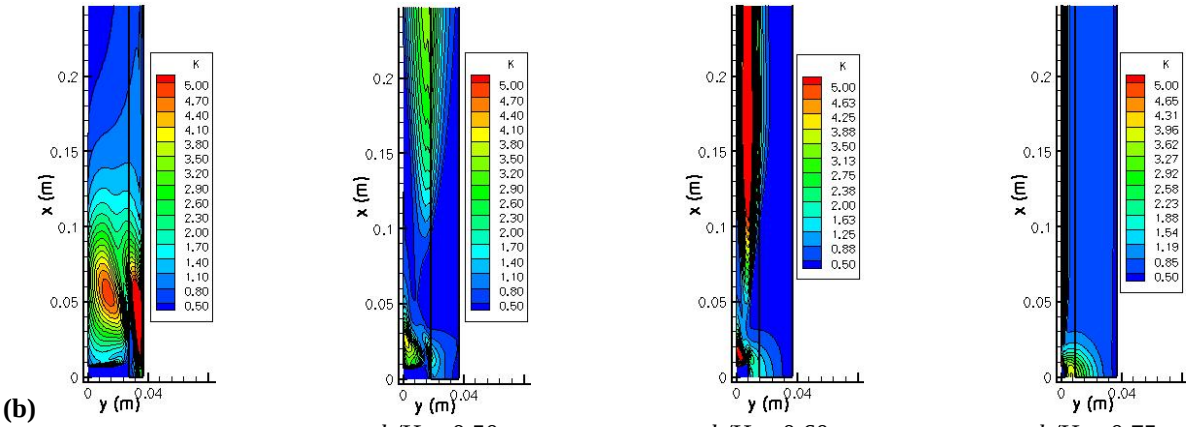


*h/H* = 0.25 *h/H* = 0.50 *h/H* = 0.60 *h/H* = 0.75

Figure 4 – Flow Behavior maps for various porous thickness layer: (a) Streamlines, (b) Turbulent Kinetic Energy

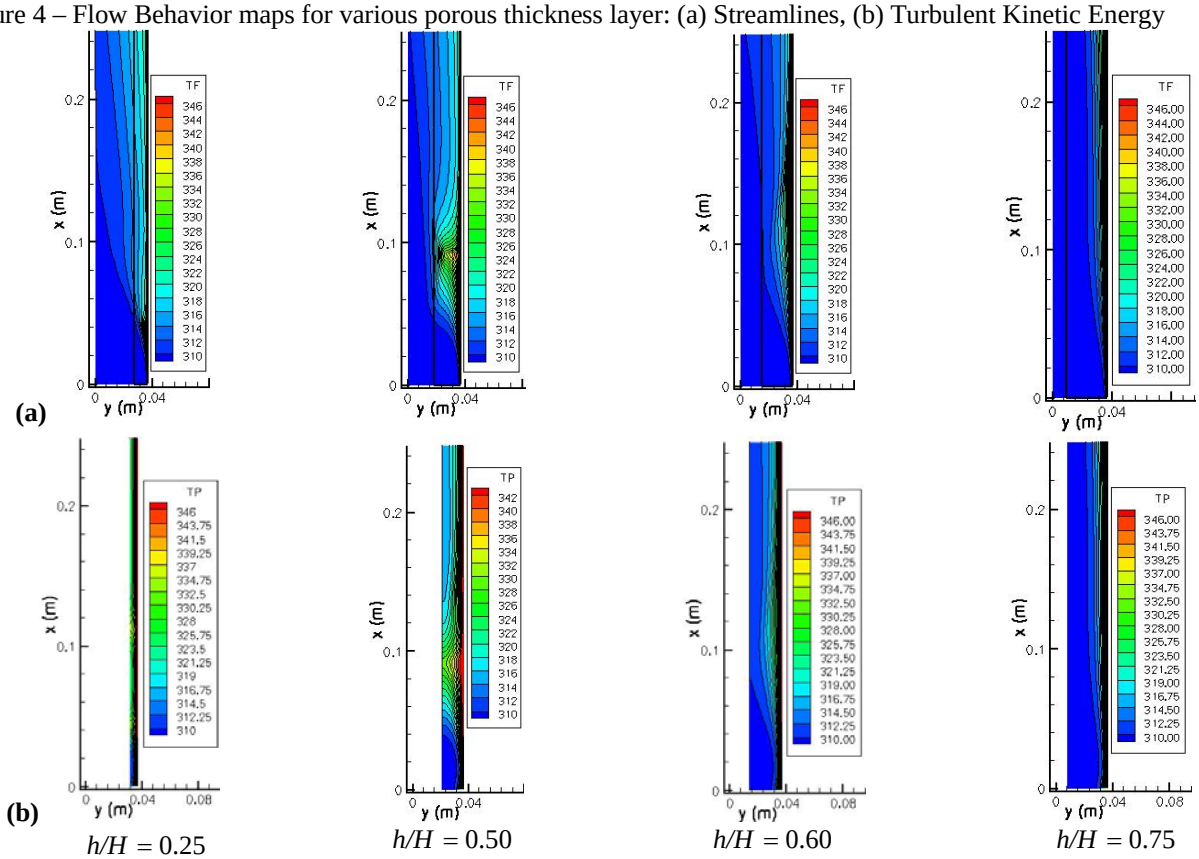


*h/H* = 0.25 *h/H* = 0.50 *h/H* = 0.60 *h/H* = 0.75

Figure 5 – Thermal Behavior maps for various porous thickness layer: (a) Fluid Temperature, (b) Solid Temperature

Figure 4a shows that porous layer thickness strongly influences the flow behavior, as also confirmed by Graminho and de Lemos (2009) and Fischer and de Lemos (2008). The primary vortex diminishes its size.as *h/H* increases. Figure4b shows that when *h/H* increases the turbulent kinetic energy decreases because the larger the porous layer the greater pressure drops in the flow. Figure 5a and Figure 5b shows that the temperature gradient decreases as *h/H* increases, since as much thinner porous bed less space has to come into equilibrium phases.

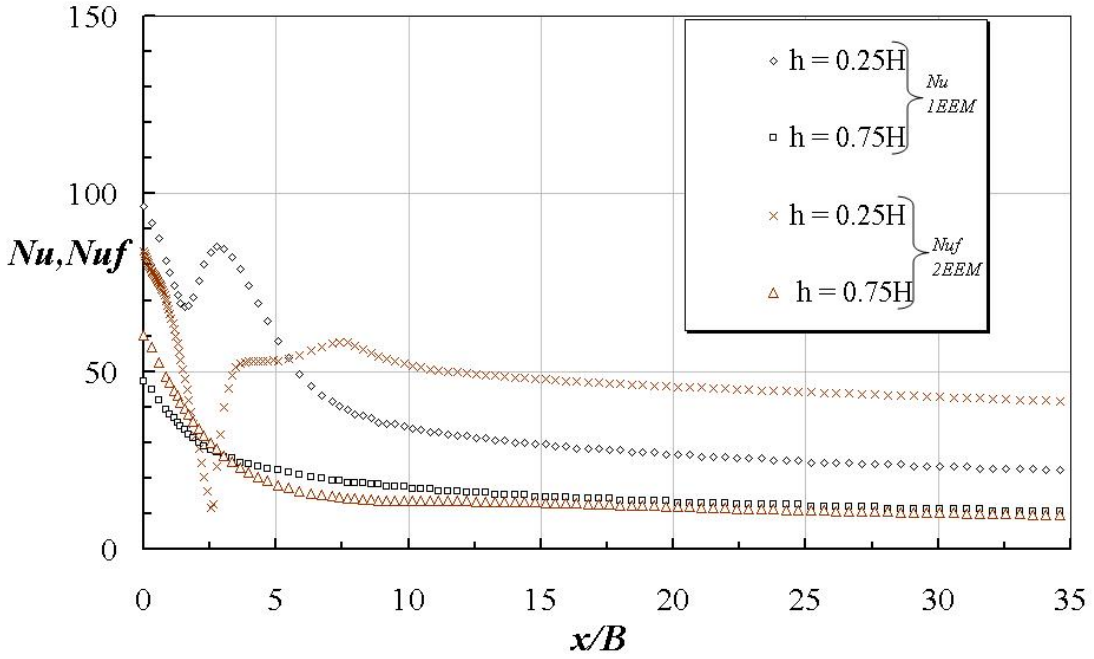


Figure 6 – Comparison of local Nusselt distribution as a function of Energy model for various porous layer thicknesses with Re=10400, $H/B = 2.6$, $k_s/k_f = 10$, (Permeability) $K = 3.31x10^{-6} m^2$ and $\phi = 0.9$

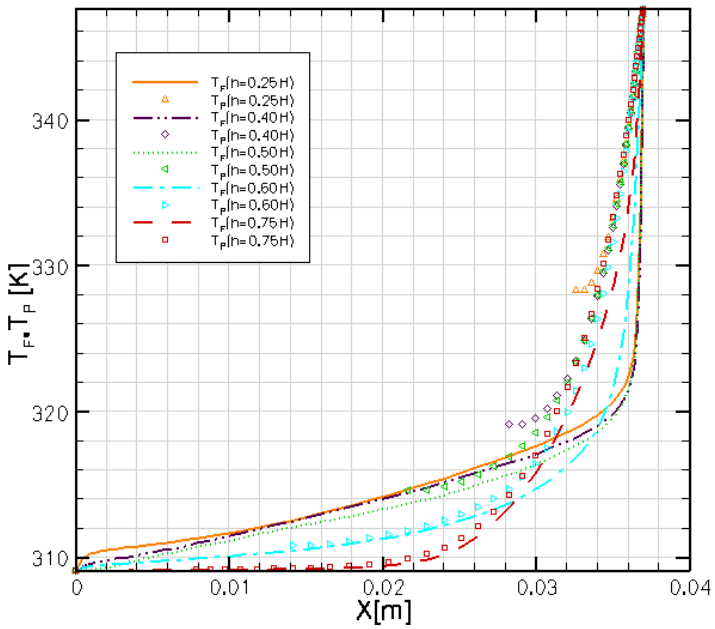


Figure 7 - Fluid and solid temperature profiles at $x/b = 2.5$ with $\mathrm{Re} = 10400$, $H/B = 2.6$, $k_s/k_f = 10$, (Permeability) $K = 3.31x10^{-6} m^2$ and $\phi = 0.9$

Figure 6 compares Nusselt number calculated with the local thermal equilibrium model (LTE) Eqn. (17) with those obtained with the local thermal non-equilibrium model (LTNE) Eqn.(19). It is observed that for porous layer thickness occupying 25% of the channel, a second peak on the local distribution of the Nusselt number is calculated for both models. For porous layer thickness occupying 75% of the channel, such peak is smoothed out when applying both models. This occur due to the fact that in such situations (low *h/H* values), temperature gradients are substantially different in both phases, as presented in Figure 7, which was plotted for the second peak location, *x/b=2.5*. Figure 7 indicates that the greater the porous layer thickness is, more intense is the heat exchange between phases and thus is more realistic consideration of Local thermal equilibrium (LTE) hypothesis.

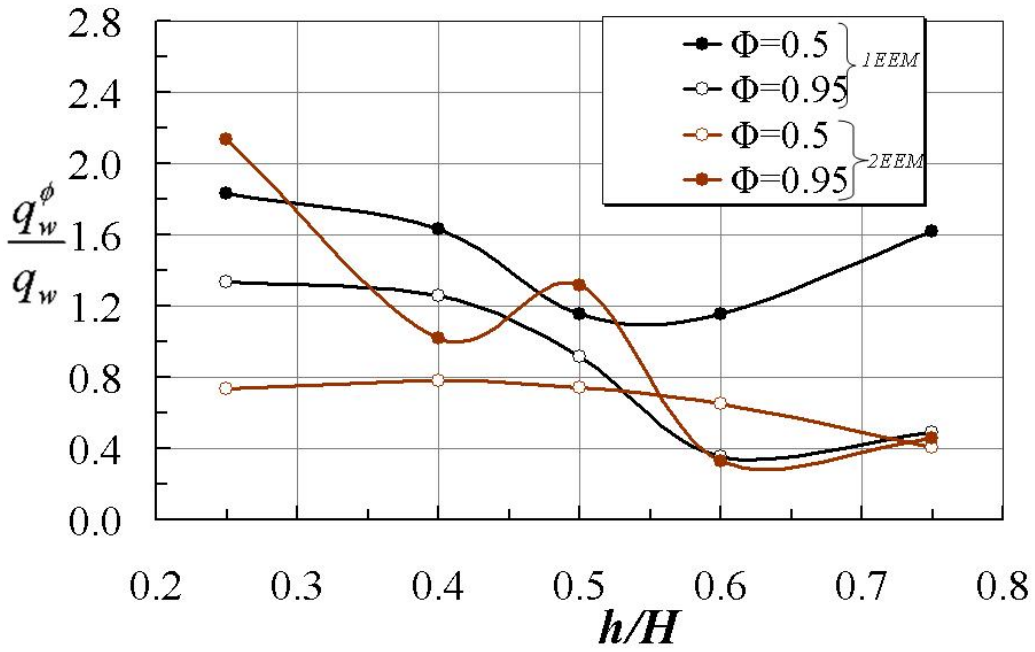


Figure 8 - Integral heat flux ratio at the lower wall for various porosities and porous layer thickness with $H/B = 2.6$, $\mathrm{Re} = 10400$, $K = 3.31x10^{-6} m^2$, $k_s/k_f = 10$. (a) $\phi = 0.5$, (b) $\phi = 0.9$

Depending on the thermal model used, there are two possibilities to evaluate the local wall heat flux $q_{wx}$. One can use the hypothesis of Local thermal equilibrium (LTE), or else, individual terms can be in each phase applied in order to calculate the integrated heat transferred from the bottom wall, in the latter case, the Local thermal non-equilibrium (LTNE) is employed.

Therefore, for one-energy equation model, one has:

$$q_w = \frac{1}{L}\int_o^L q_{wx}(x)\,dx; \quad q_{wx} = -k_{eff}\left.\frac{\partial\langle T\rangle^i}{\partial y}\right|_{y=H}; \quad k_{eff} = \phi k_f + (1-\phi)k_s \tag{26}$$

For two-energy equation model:

$$q_w = \frac{1}{L}\int_o^L q_{wx}(x)\,dx; \quad q_{wx} = -k_{eff,f}\left.\frac{\partial\langle T_f\rangle^i}{\partial y}\right|_{y=H} - k_{eff,s}\left.\frac{\partial\langle T_s\rangle^i}{\partial y}\right|_{y=H}; \quad \begin{cases} k_{eff,f} = \phi k_f \\ k_{eff,s} = (1-\phi)k_s \end{cases} \tag{27}$$

For the cases where the a porous layer is considered, the wall heat flux is given a superscript $\phi$ on the form $q_w^\phi$. The ratio $q_w^\phi/q_w$ can be seen as a measure of the effectiveness of using a porous layer for enhancing or damping the amount of heat transferred through the wall.

Figure 8 shows variations for the integral wall heat flux ratio with $h/H$ for two values of porosity $\phi$. Results indicate a substantially different ratio $q_w^\phi/q_w$ for the two models, being advantages to use ticker layer when $\phi = 0.95$. Figure 8 indicate that a presence of a porous layer has advantages, when: $\phi = 0.95$, $k_s/k_f = 10$, $h/H < 0.5$.

## 6. CONCLUSIONS

This paper investigated the behavior of an energy model, one and two energy equations model to simulate heat transfer in a turbulent impinging jet into a porous bed. Effects of porous layer thickness were investigated. The following conclusions were observed:

The presence of a porous bed on the plate eliminates the second peak in distribution of Local Nusselt number and allows for controlling heat transfer from the wall as shown Figure 6. For thinner porous layer the local Nusselt number calculated with both models is similar to free flow channel and presented the second peak in distribution, beside is observed a difference between models since as much thinner porous bed is less space has to come into equilibrium phases and therefore less realistic is the consideration of local thermal equilibrium – LTE as shown in Figure 6 and emphasized in Figure 7.

The ratio $q_w^\phi/q_w$ is less than 1 for the most of cases tested with Two energy equation model (2EEM) differently that calculated with One energy equation model (1EEM) as shown in Figure 8, since in the Two energy equation model

the heat flux were calculated with a model that consider an important aspect, the heat exchange between the solid and fluid phases or the Local Thermal Non-Equilibrium (LTNE) so the cases that passed this requirements lesser than the cases calculated with a simpler model.

Results indicates that a presence of a porous layer is beneficial for $\phi = 0.95$, $k_s/k_f = 10$ and $h/H < 0.5$, since in this conditions the ratio $q_w^{\phi}/q_w$ is greater than 1.

## 7. REFERENCES

Alazmi, Vafai, K. "Analisys of variants within the porous media transport models". Journal of Heat Transfer, 122 (2000), 303-326.

Chang K.C., Hsieh W.D., Chen C.S., "A modified low-Reynolds-number turbulence model applicable to recirculating flow in pipe expansion", Transactions of the ASME, Journal of Fluids Engineering 117 (1995) 417-423.

Fischer C.; De Lemos M.J.S. Turbulent Impinging Jet on a Plate Covered With a Porous Layer. Numerical Heat Transfer. Part A, Applications, v.58, p. 429-456, 2010.

Fox, R.W., McDonald, A.T., Introduction to Fluid Mechanics, Wiley, 5th. Ed.1998

Graminho, Daniel Rezende ; de Lemos M.J.S., "Simulation of Turbulent Impinging Jet Into a Cylindrical Chamber With and Without a Porous Layer at the Bottom". International Journal of Heat and Mass Transfer, v. 52, p. 680-693, 2009.

Hsieh W.D., Chang K.C., "Calculation of wall heat transfer in pipe-expansionturbulence flows", International Journal of Heat and Mass Transfer 39 (18) (1996) 3813-3822.

Launder, B.E., Sharma B.I., "Application of the energy-dissipation model of turbulence to the calculation of flow near a spinning disc", Letters in Heat and Mass Transfer 1 (1974) 131-138.

Launder, B.E., Spalding D.B., "The numerical computation of turbulent flows", Comp. Meth. Appl. Mech. Eng., 3 (1974) 269-289

Pedras, M.H.J., de Lemos M.J.S. "Macroscopic turbulence modeling for incompressible flow through undeformable porous media". International Journal of Heat and Mass Transfer, New York, v. 44, n. 6, p. 1081-1093, 2001.

Saito; M.B., de Lemos M.J.S., "Interfacial heat transfer coefficient for Non-equilibrium convective transport in porous media." International Communications in Heat and Mass Transfer, New York, v. 32, n. 5, p. 667-677, 2005.

Wang, S. J. Mujundar, A. S., "A comparative study of five low Reynolds number k-e models for impingement heat transfer", Applied Thermal Engineering 25 (2004) 31-44

Pedras, M.H.J., de Lemos M.J.S. "Macroscopic turbulence modeling for incompressible flow through undeformable porous media". International Journal of Heat and Mass Transfer, New York, v. 44, n. 6, p. 1081-1093, 2001.

Saito; M.B., de Lemos M.J.S., "Interfacial heat transfer coefficient for Non-equilibrium convective transport in porous media." International Communications in Heat and Mass Transfer, New York, v. 32, n. 5, p. 667-677, 2005.

Patankar, S.V., (1980)"Numerical Heat Transfer and Fluid Flow", Hemisphere, New York.

Van Heiningen A.R.P., "Heat Transfer under an impinging slot jet", Ph.D. Thesis, Department of Chemical Engineering, McGill University, Montreal, Quebec, Canada, 1982.

## 8. ACKNOWLEDGEMENTS

The authors are thankful to CAPES for their financial support during the preparation of this work

## 9. RESPONSIBILITY NOTICE

The authors are the only responsible for the printed material included in this paper.